Proactive Mobility Management With Trajectory Prediction Based on Virtual Cells in Ultra-Dense Networks

Qian Liu, Gang Chuai, Jingrong Wang, *Student Member, IEEE*, and Jianping Pan, *Senior Member, IEEE*

***Abstract*—Ultra-dense networking (UDN) is a promising technology to improve the network capacity in the next-generation mobile communication system. The virtualization paradigm is tightly integrated into UDN to address the problem of interference management. However, mobility management based on virtual cells meets significant challenges in UDN due to the frequent handovers and massive signaling overhead. These problems become severe for vehicles owing to their high-speed movement. In this paper, driven by trajectory prediction using a real-world vehicle mobility dataset, we propose a proactive mobility management solution based on virtual cells. Four modules are designed in the centralized Software-Defined Networking controller to support the proposed solution. The proposed LSTM-DR framework predicts the next locations of vehicles by integrating Long Short-Term Memory (LSTM) networks and Dead Reckoning (DR) method. The active gNBs selection algorithm selects the serving gNBs to form virtual cells according to predicted locations and mobility preferences. The corresponding signaling procedure is then carefully designed to further reduce the signaling overhead. Simulation results show that the proposed prediction framework can achieve higher accuracy and robustness in trajectory prediction. The proposed proactive solution reduces the handover frequency and handover failure rate and thereby saves the handover signaling overhead significantly.**

***Index Terms*—Proactive mobility management, trajectory prediction, mobility preference, signaling procedure, virtual cells, UDN.**

I. Introduction

Ultra-dense networking (UDN) is a pillar technology for the next-generation of mobile communication to enhance the system capacity in hotspots [1]. The ultra-dense and irregular deployment of the next-generation NodeBs, i.e., gNBs, reduces the distance between the transmitter and the receiver. With gNBs being deployed closer to users, the spectrum efficiency per unit area gets enhanced. Moreover, the ultra-dense deployment environment can bring more chances to multi-gNB cooperation. The effective utilization of radio resources among cooperative gNBs can also improve the system capacity. However, the ultra-dense gNBs deployment results in a high interference level and the degradation of communication performance.

On the other hand, virtual cell (VC) technique can take advantage of the multi-gNB cooperation to offer benefits in terms of interference management. Users receive data from multiple gNBs around them as if each user is located in the center of its own VC [2]. By this architecture, the interference sources can be turned to useful signals, and the received signals are not affected by close scattering paths. VCs enable cell-edge users to utilize resources efficiently from multiple gNBs and break the limitation of conventional static cell topology.

Instead of adopting the cell-centric approach, a user-centric VC is more suitable for UDN. On the other hand, the UDN provides more chances to realize multi-gNB cooperation. Therefore, VC technique is more tightly integrated into UDN. These two techniques were combined to improve spectral efficiency and energy efficiency [3]. However, mobility management (MM) based on VCs becomes more complicated in UDN due to the ultra-dense deployment and multi-gNB connection. Frequent handovers (HOs) may generate a large amount of control and signaling overhead, especially for users with high mobility.

N. Meng *et al.* proposed a user-centric MM solution [4], which uses VC design based on the local anchor for the seamless movement in UDN. M. Joud *et al.* adopted an adaptive cell clustering scheme accomplished with the dual connectivity technique to improve the mobility robustness in UDN [5]. The novel architectures [6], [7] were developed to support MM in UDN, which can dramatically reduce HO latency and HO overhead. These works have a similar concept of splitting control planes and user planes. They take advantage of a logically centralized control plane to maintain the connection to provide seamless coverage for mobile users.

Meanwhile, some authors proposed an SDN-based architecture in small cell networks [8], [9]. They integrated the SDN paradigm into an X2-based local MM scheme. The centralized SDN controller maintained a global view of the network. An

Manuscript received September 1, 2019; revised February 2, 2020; accepted May 5, 2020. Date of publication May 19, 2020; date of current version August 13, 2020. This work was supported in part by the National Science Technology Major Project of the Ministry of Science and Technology of China under Grant 2018ZX03001029, in part by NSERC, in part by CFI, and in part by BCKDF. The submission and revision of this paper were corresponded by Jingrong Wang, and for future communication, please correspond with Gang Chuai. The review of this article was coordinated by Dr. F. Tang. *(Corresponding author: Jingrong Wang.)*

Qian Liu is with the School of Information and Communication Engineering, Beijing University of Posts and Telecommunications, Beijing 100876, China, and also with the Department of Computer Science, University of Victoria, Victoria, BC V8W 2Y2, Canada (e-mail: liuqian@bupt.edu.cn; qianliu27@uvic.ca).

Gang Chuai is with the School of Information and Communication Engineering, Beijing University of Posts and Telecommunications, Beijing 100876, China (e-mail: chuai@bupt.edu.cn).

Jingrong Wang and Jianping Pan are with the Department of Computer Science, University of Victoria, Victoria, BC V8W 2Y2, Canada (e-mail: jingrongwang@uvic.ca; pan@uvic.ca).

Digital Object Identifier 10.1109/TVT.2020.2995318

SDN-based VC architecture was introduced [10] to enhance the quality of experience of users. These researches open a new direction to address the challenges due to the dense deployment of small cells. However, they mainly address problems of inconsistent interfaces, extensive backhauling, and seamless coverage for mobile users. The control information and signaling overhead are still frequent and massive. Moreover, most existing works target on pedestrians in UDN. Frequent HOs and heavy signaling overhead become severe if considering vehicles with higher mobility.

Therefore, the problem of frequent HOs and massive signaling overhead in UDN for the vehicle-centric VCs should be addressed. The HO procedures generally include the detection of available gNBs, the notification of VCs, the admission of resource allocation, and the execution of the HO signaling. Though the optimized HO signaling can reduce overhead to a certain degree, the frequent change of serving gNBs still causes a large amount of control information. An efficient MM solution based on vehicle-centric VCs is needed in UDN. In this paper, we analyze real-world taxi traces in Rome, Italy. These taxis are assumed located in a scenario with SDN-enabled ultra-dense networks. Each taxi adopts the user-centric VC approach to access the wireless network. A novel proactive MM solution with trajectory prediction is designed for vehicles. The main contributions of this paper are summarized as follows:

1) A trajectory prediction framework is proposed, which integrates Long Short-Term Memory networks and Dead Reckoning method to predict the vehicles' trajectories in various road scenarios.
2) Four function modules are designed for a centralized SDN controller to measure the quality of gNBs around vehicles and build VCs in advance based on the predicted locations.
3) An active gNBs selection algorithm is proposed to prioritize gNBs activation according to the mobility preferences. The proposed algorithm improves the serving time and quality of VCs and thereby reduces HO frequency and HO failure rate (HFR).
4) An HO signaling procedure is designed for VC-based MM. The optimized signaling procedure is combined with proactive management to further reduce the signaling overhead.

The rest of this paper is organized as follows. In Section II, the related work about vehicle-centric VCs, MM assisted by prediction information, and vehicle trajectory prediction is presented. In Section III, the system model and the dataset of vehicle traces are introduced. In Section IV, a proactive mobility solution is proposed. The solution includes the design of function modules, a trajectory prediction framework, an active gNBs selection algorithm, and the HO signaling procedure. The prediction and simulation results are analyzed in Section V. The conclusions are provided in Section VI.

II. Related Work

A. Vehicle-Centric VCs

Some researches are dedicated to the issue of the realizations of VCs for vehicles-to-infrastructure communications. T. Sahin *et al.* presented a realization of VCs for the vehicle broadcast groups [11]. It had improvements in terms of latency, capacity, and reliability performance. K. Chen *et al.* realized the formation of VCs by integrating open-loop radio transmission and error control [12]. It introduced a proactive network association to achieve ultra-low latency. An anticipatory MM solution was introduced to predict the next access points in the ultra-low latency communication networks [13]. However, the main target of these works is reducing latency and increasing reliability. The problem of massive signaling overhead is not solved. The serving gNBs start to provide services for vehicles after the measurement, decision, and signaling interaction procedures. These processes need a large amount of control signaling messages.

B. MM Assisted by Prediction Information

Other researches used prediction information to improve MM efficiency. The prediction algorithms were proposed [14], [15] to reduce the impact of frequent HOs on management performance and provide seamless communication. A novel prediction-based clustering scheme was proposed [16], which can predict vehicles' longevity of being the cluster head. In [17], an optimization of HO parameters was applied in UDNs to minimize the system HFR. A neural networks (NN) based model is presented in [18] to predict the next serving base stations by the sequences of Received Signal Strength (RSS). However, these works mainly focused on predicting HO, RSS, and clustering. For vehicle-centric VCs in UDN, the MM solution based on the real-world trajectory prediction has not been addressed.

Indeed, the predicted trajectories present the useful information of vehicle movement in the near future: moving direction, velocity, and mobility patterns. The information is not only useful for HO decision but also crucial for other aspects of MM, i.e., location management and resource allocation. Moreover, many taxi companies are required to install the Global Positioning System (GPS) devices in their taxis for administrative purposes, which can record the taxi traces. It provides a possibility to predict vehicles' movement by the historical trace data. Therefore, an accurate trajectory prediction is expected to help enhance the MM efficiency of vehicles, thus avoiding unacceptable degradation of the service quality.

C. Vehicle Trajectory Prediction

Vehicle mobility has a strong correlation with the inherent randomness of different drivers' driving behavior [19]. Some typical methods such as Dead Reckoning (DR) are suitable for the linear mobility pattern. Inspired by the inertia-based prediction technique, DR treats the speed and direction in the latest slot as the estimated values for the future location. The next location is calculated by the current location and the estimated speed and direction [20]. However, its performance is decreased due to the non-linear characteristic of the random movement and may lead to a large deviation [21]. Therefore, the drivers' behavior features, i.e., hidden mobility patterns, can be further extracted from the historical trajectories to improve the prediction accuracy of the near future location.

The vehicle trajectory prediction problem can be treated as a particular case of time series forecasting, which can be solved efficiently by machine learning algorithms [22]. Auto-Regressive Moving Average (ARMA) models, the traditional time series forecasting method, can be used to model the stationary trajectory series [23] and estimate vehicle positions [24]. Support Vector Machine (SVM), a supervised classification method, was also used to predict the lane change of vehicles [25], [26]. The Random Forest (RF) model has been shown to have a better trajectory prediction accuracy than the Kalman filter [27], as well as being robust in predicting latitude and longitude [28]. However, compared with the Recurrent Neural Network (RNN), the traditional machine learning methods could result in a high computational cost and lower prediction accuracy for long-term time series [29]–[31].

RNN is especially suitable to capture the temporal and spatial evolution of human moving patterns [32]. Long Short-Term Memory (LSTM) networks, a typical RNN architecture, is designed to learn the long-term time series. It is able to store and update the key information efficiently over a long time. LSTM networks are considered particularly efficient for time series forecasting [33], [34] and have been widely used in the vehicle trajectory prediction [35]–[37]. Regarding the city-wide mobility, we have observed that NN-based methods maintain high accuracy in complex traffic environments such as downtown, while DR-based methods show the superiority of low computation complexity on highways. In this paper, we not only leverage the advantage of LSTM but also jointly consider the road limitations. The proposed LSTM-DR integrated prediction framework can handle various road and traffic scenarios.

From the related work listed above, it can be found that the vehicles' trajectories can be predicted efficiently, and the predicted information is beneficial for vehicles' MM. If HO can be prepared in advance and the appropriate serving gNBs are selected according to the predicted locations, the number of HOs and the signaling cost can be reduced significantly. Therefore, a VC-based proactive management solution is proposed for vehicles, which reasonably selects the serving gNBs in advance based on the predicted trajectories.

III. System Model

An SDN-enabled ultra-dense network is illustrated in Fig. 1. The network consists of an SDN controller and multiple gNBs with vehicles driving along the road. The controller manages all gNBs to provide wireless access for vehicles. gNBs $\mathcal{I}$ are distributed subject to a stationary Poisson Point Process (PPP) with density λ. A set of gNBs within radius D around vehicle $j \in \mathcal{J}$ form a VC. Therefore, the candidate gNBs of vehicle j can be denoted as $V_j = \{i \in \mathcal{I} \ s.t.\ d_{ij} \le D\}$, where d_{ij} is the Euclidean distance between gNB i and vehicle j.

gNBs in V_j are considered as "active" when their reference signal received power (RSRP) are higher than a threshold T. The active gNBs provide services to vehicle j simultaneously by the non-coherent joint transmission (NCJT) mechanism. An indicator $a_{ij} \in \{0, 1\}$ reflects whether gNB i is activated for vehicle j or not.

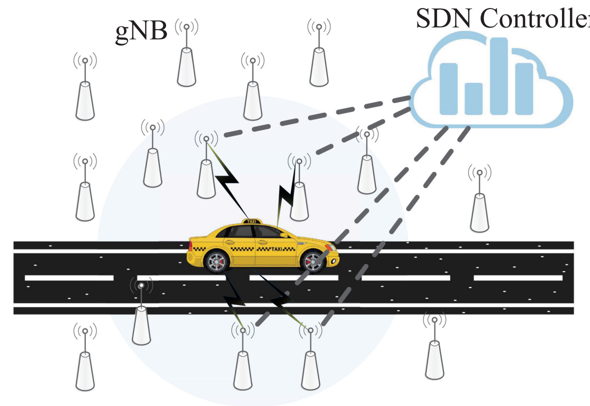

Fig. 1. Network architecture.

Each channel between gNBs and vehicles is assumed independent. The channel gain between gNB i and vehicle j is

$$h_{ij} = \sqrt{l_{ij}} f_{ij}, \tag{1}$$

where f_{ij} is the fading gain following a unit-mean exponential distribution (Rayleigh fading). $l_{ij} = |d_{ij}|^{-\alpha}$ is the path-loss and $\alpha > 2$ is the pass-loss exponent.

A. Communication Model

The channel state information (CSI) is assumed imperfect in this paper, and the error introduced by channel estimation is treated as a new interference. Therefore, the signal-to-interference-plus-noise ratio (SINR) of vehicle j is

$$\gamma_j = \frac{\sum_{i \in V_j} P_i |h_{ij}|^2 a_{ij} \left(1 - {\sigma_{ij}}^2\right)}{\sum_{i \in V_j} P_i |h_{ij}|^2 a_{ij} {\sigma_{ij}}^2 + \sum_{i \in \overline{V}_j} P_i |h_{ij}|^2 + \eta}, \tag{2}$$

where P_i is the transmitted signal power from gNB i, and η is the white noise power. σ_{ij}^2 is the minimum mean-square error of the channel estimation between gNB i and vehicle j, which can be calculated as [38].

$${\sigma_{ij}}^2 = \frac{1}{1 + \frac{|h_{ij}|^2}{\sum_{i \in V_j} |h_{ij}|^2 + \eta / P_i} \frac{N}{U_j}}, \tag{3}$$

where N is the total number of resource blocks in the pilot-based channel estimation, and U_j is the number of active gNBs in V_j.

According to (16) and (17) in [39], the average spectral efficiency $E[C_j]$ can be calculated [40] as

$$\begin{aligned} E[C_j] &= \int_0^\infty P(\gamma_j > 2^x - 1) dx \\ &= \int_0^\infty (1 - P(\gamma_j \le 2^x - 1)) dx, \end{aligned} \tag{4}$$

$C = \log_2(1 + \gamma_j)$. Let $\beta = 2^x - 1$, we can obtain $x = \log_2(\beta + 1)$. $E[C_j]$ can be further derived as

$$\begin{aligned} E[C_j] &= \int_0^\infty (1 - P(\gamma_j \le \beta)) d(\log_2(\beta + 1)) \\ &= \frac{1}{\ln 2} \int_0^\infty \frac{1}{\beta + 1} (1 - P(\gamma_j \le \beta)) d\beta, \end{aligned} \tag{5}$$

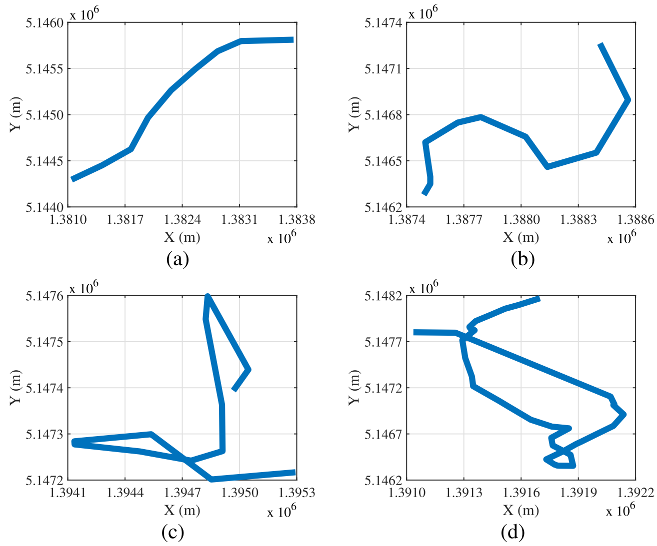

Fig. 2. Trajectory patterns. (a) Smooth curves (P1). (b) Making turns (P2). (c) Making U-turns (P3). (d) Circling around (P4).

where β is an SINR threshold. Thus, $E[C_j]$ can be calculated by SINR distribution, which can be approximated as

$$P(\gamma_j \leq \beta) = (\kappa - \lfloor\kappa\rfloor)\mathcal{L}_p^{(\lceil\kappa\rceil)}(\frac{1}{\theta\beta})\frac{(\theta\beta)^{-\lceil\kappa\rceil}}{\lceil\kappa\rceil!} + \sum_{m=0}^{\lfloor\kappa\rfloor}\mathcal{L}_p^{(m)}(\frac{1}{\theta\beta})\frac{(\theta\beta)^{-m}}{m!}, \tag{6}$$

where $\mathcal{L}_p$, κ and θ can be obtained in [41].

B. Dataset of Vehicle Traces

The real-world vehicle traces [42] in Rome, Italy, are used to illustrate vehicle mobility. It consists of the GPS trajectories of 320 taxis from 1st February 2014 to 2nd March 2014. Each vehicle's trace includes a list of GPS coordinates (longitude and latitude) and the corresponding timestamps. The sample interval of the GPS coordinates is 15 s. The distances between adjacent coordinates are extracted as an input for the proposed prediction framework. The trajectories are divided into four patterns according to their main features: smooth curves (P1), making turns (P2), making U-turns (P3), and circling around (P4), which are as shown in Fig. 2.

IV. Proactive Mobility Management Solution

A novel proactive MM solution is proposed to reduce the signaling cost and enhance HO performance. Generally, vehicles measure RSRPs from gNBs and send the measurement reports to the SDN controller. The controller makes HO decisions based on the received measurement reports and the predicted trajectories of vehicles. More specifically, the proposed MM solution is described in the following aspects: 1) function modules of MM; 2) an LSTM-DR integrated prediction framework; 3) an active gNBs selection algorithm, and 4) an HO signaling procedure.

A. Function Modules of MM

In the SDN controller, four function modules are designed for the proactive MM solution. These modules are in charge of prediction control, measurement control, HO control, and admission control.

1) Prediction Control Module: This module is in charge of vehicle trajectory prediction. The LSTM-DR integrated framework predicts the next location of a vehicle using its historical trajectories. Details can be found in Section IV-B.

2) Measurement Control Module: Based on the prediction locations, the SDN controller detects candidate gNBs in the corresponding region, and measures the states of the candidate gNBs.

The measurement region is expanded to mitigate the impact of prediction deviations on HO performance. The radius of measurement regions is expanded from D to R.

$$R = D + \delta, \tag{7}$$

where δ is the median of mean absolute errors of all vehicles' prediction trajectories. The measurement contents include the specific states of gNBs: ID and available spectrum resources.

3) HO Control Module: The HO decision-making procedure is triggered by event A2 with a threshold C_{m}, i.e.,

$$C_j^t < C_{\mathrm{m}}, \tag{8}$$

where C_j^t is the system spectral efficiency of vehicle j at time t. $C_{\mathrm{m}} = \epsilon_{\mathrm{m}} \times E[C_j]$ is the threshold in event A2, which is higher than the minimum required capacity. ϵ_{m} is the proportional value of the threshold relative to $E[C_j]$.

After HOs are triggered, a set of active gNBs are selected from candidate gNBs by the proposed active gNBs selection algorithm described in Section IV-C. Then, the new list of active gNBs A_j^{t+1} is sent to the vehicle after a time-to-trigger (TTT) time. Compared to the old activation list A_j^t, these gNBs are divided into three categories: new gNBs, old gNBs, and ongoing gNBs. New gNBs need to be added to VC, old gNBs are deleted from VC, and ongoing gNBs maintain their connection. An HO signaling procedure is designed to support the VC-based HO, and its details can be found in Section IV-D.

4) Admission Control Module: This module guarantees the candidate gNBs sufficient spectrum resources for data transmission. The controller removes a gNB in the overloaded condition from the activation list, and the newly available gNB will be added.

B. The LSTM-DR Integrated Prediction Framework

In the prediction control module, an LSTM-DR integrated prediction framework is proposed by taking advantage of LSTM and DR to handle various road and traffic scenarios.

1) Framework Construction: In the proposed prediction framework, the vehicle's trajectory and the extracted distances are fed into an LSTM neural network. The outputs are the directions and distances in the next time interval. A three-layer LSTM neural network is established with the first layer of 20 neurons, the second layer of 50 neurons, and the third dense layer. The previous 19 locations are used to predict the next location. Then, the final predicted location can be generated by the predicted direction, distance, and the current location according to the DR method.

2) Evaluation Metrics: The Mean Haversine Distance (MHD) ζ_{jk} is used to calculate the deviation of vehicle j between the predicted GPS coordinate $(\widehat{\omega_{jk}}, \widehat{\mu_{jk}})$ and real coordinate (ω_{jk}, μ_{jk}). $k \in \mathcal{K}_j$ (with $K_j = |\mathcal{K}_j|$) represents the index of sample locations on vehicle trajectories.

$$\zeta_{jk} = 2 \times r \times \arctan\left(\sqrt{\frac{\rho}{1-\rho}}\right), \tag{9}$$

$$\rho = \sin^2\left(\frac{\widehat{\omega}_{jk} - \omega_{jk}}{2}\right) + \cos(\widehat{\omega}_{jk})\cos(\omega_{jk})\sin^2\left(\frac{\widehat{\mu}_{jk} - \mu_{jk}}{2}\right), \tag{10}$$

where $r = 6,371$ km is the radius of the Earth's sphere.

Mean absolute error (MAE) and root mean square error (RMSE) are used to evaluate the prediction accuracy of vehicle j with K_j predicted locations.

$$MAE_j = \frac{1}{K_j}\sum_{k=1}^{K_j}\zeta_{jk}, \tag{11}$$

$$RMSE_j = \sqrt{\frac{1}{K_j}\sum\nolimits_{k=1}^{K_j}{\zeta_{jk}}^2}. \tag{12}$$

After taking the average over $J = |\mathcal{J}|$ vehicles, the average MAE (AMAE) and the average RMSE (ARMSE) can be obtained as

$$AMAE = \frac{\sum_{j=1}^{J} MAE}{J}, \tag{13}$$

$$ARMSE = \sqrt{\frac{\sum_{j=1}^{J} RMSE^2 K_j}{\sum_{j=1}^{J} K_j}}. \tag{14}$$

C. Active gNBs Selection Algorithm

In the VC-based UDN, a vehicle is served by multiple gNBs. When the vehicle's communication capacity falls below a threshold, the controller needs to select new serving gNBs for it. Based on our observation, the priorities of gNBs selection are associated with not only their channel qualities but also the vehicle's moving direction and velocity. On the one hand, the gNB located in the vehicle's moving direction has a higher priority to serve the vehicle [17]. On the other hand, the resident time of the vehicle served by a certain gNB is affected by its velocity [43]. The gNBs with a short serving time will result in frequent HOs. Therefore, the gNBs located in the moving direction are preferred to be activated, which have a longer average serving time.

The intuition of the proposed gNBs selection algorithm is illustrated in Fig. 3. When the vehicle is stationary, the measurement region is a circular area with radius R, which is shown in blue line. As the velocity increases, the measurement region will be more biased toward the moving direction, which is shown in solid red line. This intuition is to prolong gNB/VC serving time to reduce HO frequency. If a longer service time is pursued blindly, the selected gNBs will be excessively biased toward the moving direction, thereby the vehicle's quality of service (QoS) significantly degrades at the current location. When the vehicle's capacity at the current location is lower than C_{m}, event A2 is triggered again. Therefore, the blindly sacrificed capacity does not result in a drop of the HO frequency and even brings in additional HOs. A threshold is set to avoid the excessive capacity reduction, i.e., the adjusted measurement region should provide the vehicle with a capacity that is larger than C_{m} at the current location. As shown in Algorithm 1, an active gNBs selection algorithm is proposed following this intuition to select serving gNBs for vehicles.

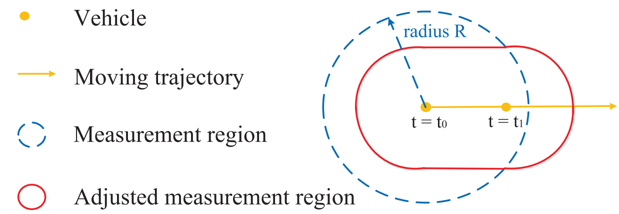

Fig. 3. Measurement region with selection preference.

First, the controller sets a circular protection area for each vehicle with radius $\widehat{R_j}$. $\widehat{R_j}$ depends on the velocity v_j of vehicle j, which is calculated as

$$\widehat{R}_j = R - \left(\frac{v_j}{v_{\max}}\right) \times (D_{\mathrm{opt}} - D_{\mathrm{m}}), \tag{15}$$

where $v_{\max}$ is the highest speed limit of taxis in Rome. D_{opt} is the optimal D, which maximizes $E[C_j]$. D_{m} is the VC radius corresponding to C_{m} [41]. The protection radius $\widehat{R}_j$ is related to v_j. When the velocity is low, the probability of frequent HO is relatively low. Sacrificing too much capacity for a longer VC serving time is not expected. A large protection radius can provide a good QoS for the vehicle to avoid the HO failure at the current location. As the velocity increases, the probability of HO is increasing accordingly. Therefore, the primary goal of MM turns to reduce the HO frequency, and thereby the controller prefers to activate gNBs located in the moving direction. As a result, a small protection radius is needed for high velocity.

Next, the controller calculates the length of the vehicle's trajectory in the adjusted measurement region with selection preference. For computation convenience, an ellipse is used to approximate the adjusted region and assume that vehicles are traveling in straight lines between the adjacent sample locations. Let L_j denote the trajectory of vehicle j in the adjusted measurement region. The total number W_j of sample locations of vehicle j on L_j is counted by the controller. For each gNB $i \in V_j$, the average distance between it and W_j sample locations is calculated as

$$E[d_{ij}] = \frac{1}{W_j}\sum_{t=1}^{W_j} d_{ij}^{(t)}. \tag{16}$$

Finally, U_j gNBs are chosen from the candidate gNBs with the shortest $E[d_{ij}]$ to serve the vehicle. For a fair comparison, U_j stays the same as the number of serving gNBs in the reactive solution at the corresponding predicted locations [41].

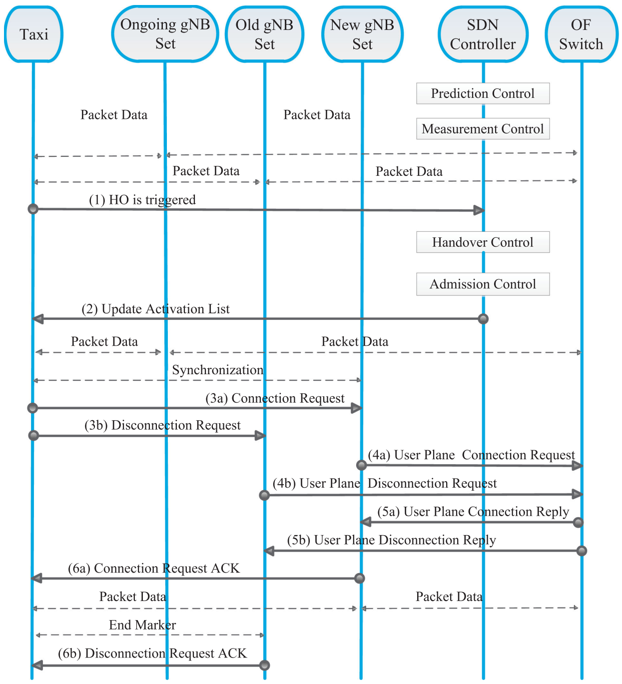

Fig. 4. Proactive HO signaling procedure.

Algorithm 1: Active gNBs Selection.

Input:
the current location (ω_{jk}, μ_{jk}),
the predicted location $(\widehat{\omega_{jk}}, \widehat{\mu_{jk}})$,
the locations of gNBs,
the radius of measurement region R,
the measurement report,
the old activation list A_j^t.
Output:
the new activation list A_j^{t+1}.

A2: $C_j^t < C_{\mathrm{m}}$;
if *A2 is satisfied* **then**
  report candidate gNBs V_j by R and $(\widehat{\omega_{jk}}, \widehat{\mu_{jk}})$;
  calculate the number of active gNBs U_j by D and $(\widehat{\omega_{jk}}, \widehat{\mu_{jk}})$;
for $i \in V_j$ **do**
  calculate $E[d_{ij}]$ by (16)
  ;
sort gNB $i \in V_j$ in ascending order of $E[d_{ij}]$;
select the first U_j gNBs to form the new activation list A_j^{t+1};
return A_j^{t+1};

D. HO Signaling Procedure

The HO signaling procedure is designed to support HOs based on VC, and its main steps are illustrated in Fig. 4.

Step 1: HO is triggered when event A2 is satisfied.

TABLE I
SYSTEM PARAMETERS IN THE SIMULATION

Parameter	Value	Parameter	Value
λ_{gNB}	174 / km^2	N	92
D_{opt}	0.122 km	ϵ_m	0.35
T	0 dBm	$v_{\max}$	130 km/h
α	4	$T_{\mathrm{OF-Switch}}$	50 ms [8]
P_i	30 dBm	P_{gNB}	4 ms [8]
η	-174 dBm/Hz	$P_{\mathrm{SDN-Controller}}$	15 ms [8]

Step 2: The controller executes HO control and admission control. Then, it sends the new activation list of gNBs A_j^{t+1} to vehicle j after a TTT time.

Step 3: The vehicle receives A_j^{t+1} and divides gNBs in A_j^{t+1} into three classes as mentioned above. Then, it sends connection requests and disconnection requests simultaneously to new gNBs and old gNBs, respectively.

Step 4: The new gNBs transmit connection requests to the OpenFlow (OF) switch. At the same time, the old gNBs transmit disconnection requests to the switch.

Step 5: The switch sends replies to new gNBs and old gNBs, respectively.

Step 6: The new gNBs send connection acknowledgments (ACKs) to the controller. Then they build connections with the vehicle and transfer the data. Meanwhile, the old gNBs send ACKs to the controller and detach data paths from the vehicle. The ongoing gNBs transfer the buffered data continuously.

V. Numerical Results

The proposed solution selects the serving gNBs for a vehicle based on its measurement report and predicted locations, and then starts the HO process in advance. In this section, the prediction results of the LSTM-DR integrated framework are compared with other state-of-the-art methods. Then, the management performance of the proposed solution is evaluated in terms of HFR, HO signaling time, and message cost. The simulation parameters are shown in Table I.

A. Prediction Results

The proposed LSTM-DR integrated framework is evaluated on the platform of an Intel (R) Core (TM) i7-3770 CPU @ 3.40 GHz. The default prediction interval is 15 seconds, which is the same as the minimum sample interval in the historical traces. Vehicles are divided into four patterns mentioned in Section III-B according to the main feature of their predicted trajectories. 96 taxis are chosen to guarantee that there are enough taxis in each mobility pattern.

The performance of different prediction methods on four trajectory patterns is shown in Table II. AMAE and ARMSE are used together to diagnose the variation of trajectory prediction. Since the errors are squared before they are averaged, ARMSE gives a relatively high weight to large errors. Generally, the larger the difference between ARMSE and AMAE is, the larger the prediction errors exist. It can be seen that LSTM-DR has the highest accuracy on ARMSE. Although DR has a similar performance with LSTM-DR on AMAE, the gap between AMAE

TABLE II
PERFORMANCE AMONG DIFFERENT PATTERNS

Model	Metric (km)	Trajectory pattern				Average
		P1	P2	P3	P4	
LSTM-DR	AMAE	0.063	0.070	0.072	0.075	0.070
	ARMSE	**0.254**	**0.263**	**0.392**	**0.386**	**0.324**
DR	AMAE	**0.047**	**0.058**	**0.060**	**0.065**	**0.058**
	ARMSE	0.343	0.471	**0.614**	**0.576**	0.501
LSTM	AMAE	0.256	0.266	0.271	0.293	0.272
	ARMSE	0.306	0.443	0.562	0.540	0.463
ARMA	AMAE	1.588	1.899	2.282	1.874	1.911
	ARMSE	2.589	2.816	4.501	2.592	3.125
RF	AMAE	3.763	2.955	2.920	2.948	3.147
	ARMSE	5.396	3.911	4.232	3.530	4.267
SVM	AMAE	4.161	4.767	5.507	5.459	4.974
	ARMSE	4.721	5.386	6.036	6.178	5.580

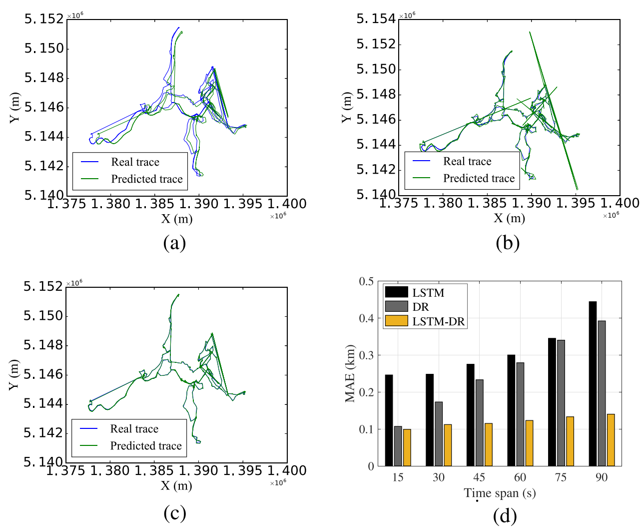

Fig. 5. Prediction performance. (a) LSTM. (b) DR. (c) LSTM-DR. (d) Impact of time span on MAE.

and ARMSE of DR is 74.4% larger than that of LSTM-DR. This indicates that large prediction deviations happen at certain points by DR. Overall, the proposed LSTM-DR model has stable and robust prediction performance.

Taking taxi 2 as an example, the comparison between the predicted and real trajectory regarding the three methods are shown in Fig. 5(a), (b), and (c), respectively. It can be seen that the predicted trajectory of LSTM-DR has the best match with the real trajectory. DR has a large deviation in some predicted points. However, LSTM has a high consistency with the real trace especially when the taxi makes turns. The impact of different time spans on the prediction performance is shown in Fig. 5(d). MAEs of the three prediction methods (LSTM, DR, and LSTM-DR) increase with the growth of the time span. For all methods, the prediction result under 15 seconds is more accurate than those over other spans. Moreover, the LSTM-DR integrated framework is shown to be more robust over different time spans.

The proposed LSTM-DR integrated framework does not require any special hardware such as GPUs. The time cost of the framework is demonstrated in Table III. The training time of the

TABLE III
TIME COST

# of sample locations	1000	3000	5000	7000
Training time (s)	176.72	530.12	833.21	1236.06
Prediction time (s)	0.12	0.37	0.61	0.83

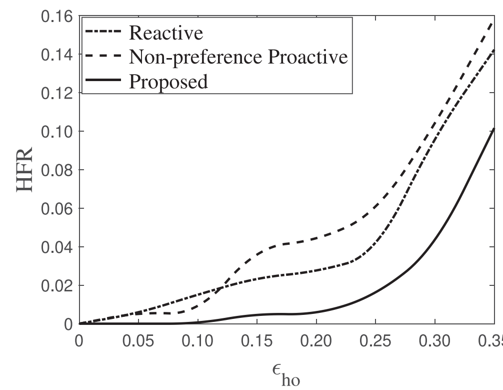

Fig. 6. HFR of different MM solutions.

proposed prediction architecture is acceptable, and its prediction time is short.

B. MM Results

In this subsection, the management performance of the proposed MM solution is compared with the reactive solution [10] and the non-preference proactive solution [44]. In the reactive solution, VCs are frequently updated as the vehicle moves, and HOs are triggered when VCs changed. For the non-preference proactive solution, only the LSTM model is used for trajectory prediction, and all gNBs in VCs are activated to provide services without selection preference.

1) HFR: HO failure occurs when the received capacity of the vehicle is less than a capacity threshold C_{ho}.

$$C_j^t < C_{\mathrm{ho}}, \tag{17}$$

where $C_{\mathrm{ho}} = \epsilon_{\mathrm{ho}} \times E[C_j]$. ϵ_{ho} is the proportional value of the threshold relative to the average spectral efficiency $E[C_j]$. It represents the capacity requirement of a successful HO and is no greater than ϵ_{m}. In this work, we do not differentiate when HO failure occurs. HFR is calculated as

$$\mathrm{HFR} = \frac{\#\text{ of HO failures}}{\#\text{ of HOs}}. \tag{18}$$

Fig. 6 shows the impact of ϵ_{ho} on HFRs of different MM solutions. With the increase of ϵ_{ho}, the capacity requirement becomes strict. When ϵ_{ho} is lower than 0.12, the reactive solution has the highest HFR, and the non-preference proactive solution can reduce the HFR by up to 50%. It is because the proactive solution executes the HO preparation based on the trajectory prediction in advance. It avoids the impact of invalid measurement due to the movement of vehicles and HO delay and thus leads to a lower HFR. The proposed solution further reduces HFR by the efficient gNBs selection algorithm. The optimization of gNBs selection gives its VCs a longer average serving time.

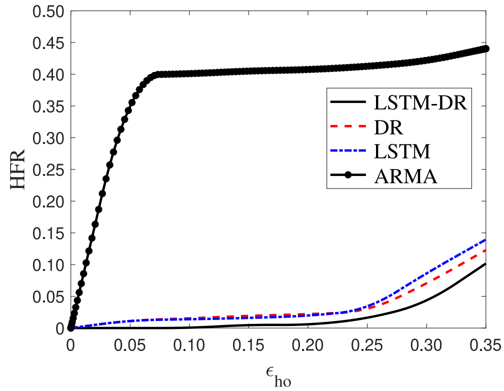

Fig. 7. HFR of different prediction methods.

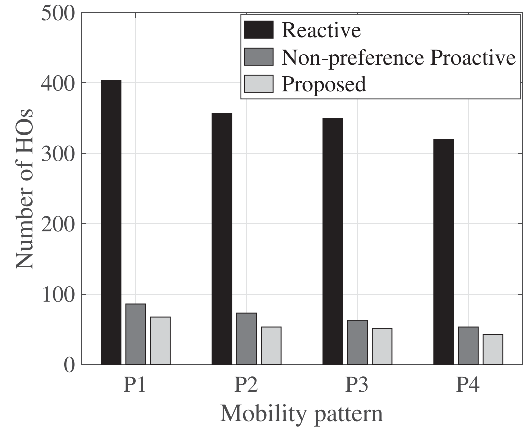

Fig. 8. Number of HOs for different MM solutions.

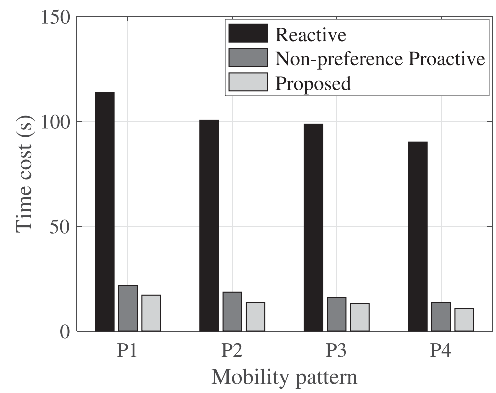

Fig. 9. Time cost of different MM solutions.

Besides, HOs are triggered only when event A2 is satisfied. These designs greatly reduce the number of unnecessary HOs, and thereby avoid the potential HO failure. Therefore, the HFR of the proposed solution is the lowest.

With ϵ_{ho} increasing from 0.12 to 0.35, the HFR of the non-preference proactive solution becomes the highest. The main reason is that the prediction deviation results in a lower capacity in certain places, especially when taxis change their direction sharply. However, the proposed solution can maintain a low HFR, since the measurement region is enlarged to mitigate the impact of the prediction deviations. Then, the selection of serving gNBs is optimized by selection preference. It can avoid HO failures caused by the large prediction deviations. A proper capacity threshold of HO failure is vital for HFR performance. Overall, the proposed solution has the best performance on HFR compared to other MM solutions.

Fig. 7 shows the impact of ϵ_{ho} on HFRs regarding different prediction methods. The default MM solution is the proposed proactive solution with selection preference. ϵ_{ho} is the proportional value of the threshold relative to the average spectral efficiency $E[C_j]$, which represents the capacity requirement for a successful HO. It can be seen HFRs based on four prediction methods all increase with the growth of ϵ_{ho}. This is because the stricter the criterion of successful HOs is, the higher the probability of HO failure becomes. Moreover, an accurate location prediction helps enhance HO decision-making. Under the same MM solution, the MM performance is mainly affected by the prediction performances. When ϵ_{ho} is small, the MM performance is in accordance with ARMSE. As the system has a higher tolerance to prediction errors, the MM performance is mainly affected by very large prediction deviations, which are evaluated by ARMSE. When ϵ_{ho} is large, HFR is sensitive to both ARMSE and AMAE. Overall, LSTM-DR maintains the lowest HFR when compared to other methods. It is because LSTM-DR takes advantage of both LSTM and DR as well as avoiding large prediction deviations.

2) HO Number: HO frequency is affected by the HO triggering condition and the serving time of VCs. Fig. 8 shows the total number of HOs under different mobility patterns regarding different MM solutions. In the reactive solution, VCs are frequently updated as the vehicle moves, thus resulting in high HO frequency. When compared with the non-preference proactive solution, the proposed proactive solution jointly considered the impact of trajectory on gNB selection as well as a flexible measurement region. Overall, the number of HOs under the proposed solution remains the lowest among the three MM solutions.

3) HO Cost: The HO cost mainly includes two parts: the time cost and the message cost.

The time cost S_t is defined as the HO processing time in the whole simulation area, and it is calculated by the number of HOs N_{ho} and the HO signaling processing time $\mathcal{T}$. $\mathcal{T}_{\mathrm{pro}}$ and $\mathcal{T}_{\mathrm{rea}}$ can be obtained from Fig. 4 and [10], separately.

$$S_t = N_{\mathrm{ho}} \times \mathcal{T}, \tag{19}$$

$$\mathcal{T}_{\mathrm{pro}} = 4T_{\mathrm{OF-Switch}} + 6P_{\mathrm{gNB}} + 2P_{\mathrm{SDN-Controller}}, \tag{20}$$

$$\mathcal{T}_{\mathrm{rea}} = 4T_{\mathrm{OF-Switch}} + 13P_{\mathrm{gNB}} + 2P_{\mathrm{SDN-Controller}}, \tag{21}$$

where $T_{\mathrm{OF-Switch}}$ is the transmission latency between gNB and the OpenFlow-enabled switch, P_{gNB} is the processing latency at gNBs, and $P_{\mathrm{SDN-Controller}}$ is the latency at the SDN controller. The time costs of four patterns are shown in Fig. 9.

According to (18), HO time cost S_t is affected by both the number and execution time of HO. When comparing the proposed HO signaling procedure with the reactive solution,

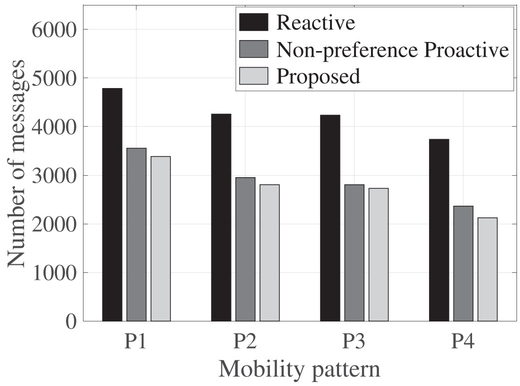

Fig. 10. Message cost of different MM solutions.

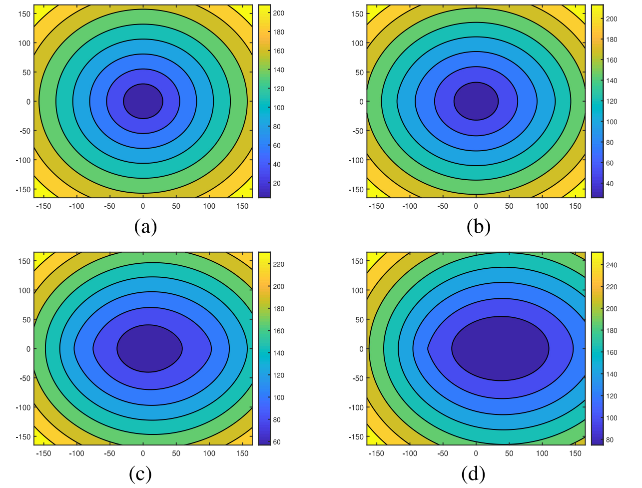

Fig. 11. The impact of velocity on the adjusted VC region. (a) velocity = 0 m/s. (b) velocity = 6 m/s. (c) velocity = 18 m/s. (d) velocity = 30 m/s.

our approach has a shorter execution time. It simultaneously executes the process of activating new gNBs and releasing old gNBs (Step 3, 4, 5, and 6 in Fig. 4). Thereby, $\mathcal{T}_{\text{pro}}$ can save 10% HO execution time when compared with $\mathcal{T}_{\text{rea}} = 0.282$ s. Besides, the two proactive solutions reduce the HO frequency significantly by the proper gNB selection based on the precise trajectory prediction. The proposed solution with mobility preference can further reduce the HO frequency due to a longer serving time of the adjusted VC. Therefore, the proposed solution can efficiently decrease HO cost.

In the same duration (450 s), the cumulative HO time costs of all solutions decrease gradually from P1 to P4. As the areas taxis passing through shrink, a fewer number of HO and signaling costs are needed. On the other hand, the gaps between two proactive solutions also decrease from P1 to P4. The trajectory prediction accuracy decreases when taxis make more turns, thus resulting in performance degradation. Ultimately, under different mobility patterns, the proposed solution can efficiently reduce the HO time cost.

The message cost S_m is the total signaling messages involved in the HO process, and it is calculated by the N_{ho} and the signaling message involved in each HO procedure. The message cost can be calculated as

$$S_m = \sum_{ho=1}^{N_{\text{ho}}} (2 + 4\mathcal{M}_{\text{ho}}), \tag{22}$$

where $\mathcal{M}_{\text{ho}}$ is the number of new and old gNBs in an HO process, and its value is different in each HO process.

The message costs of four trajectory patterns are shown in Fig. 10. From (21), it can be seen that the cumulative HO message costs of three management solutions decrease from P1 to P4 in the same duration (450 s). From the above analysis, it can be found that two proactive solutions can reduce the number of HO significantly. Furthermore, the total number of new and old gNBs in the HO process is decreased by the proposed gNBs selection algorithm. By considering the impact of moving direction and velocity, the gNB selection becomes more targeted and efficient. Therefore, unnecessary gNBs are deleted from the new VC, and the number of exchanged messages decreases. The proposed solution has the least message cost for all mobility patterns.

4) The Adjusted VC Region: From the analysis in Section IV-C, the VC region is adjusted according to the gNBs selection preferences, which is affected by the predicted direction and the vehicle's velocity. According to the intuition in Fig. 3, the adjusted VC regions on different velocities are shown in Fig. 11. It can be seen that the adjusted VC region changes from the circle area to the approximate ellipse with the increase of velocity. Moreover, the ellipse drifts in the moving direction, and the change is increasing with the vehicle's velocity. However, the change requires careful control. If the ellipse is drifted too much in the direction, it will directly affect the capacity after HO. The decrease in capacity will cause HO failure. If the change is small, the serving time of VC cannot be effectively extended.

VI. Conclusion

In this paper, a proactive mobility management solution based on VC technique is proposed. The SDN controller proactively manages HO processes of vehicles based on the trajectory prediction. An LSTM-DR integrated prediction framework was designed to improve prediction accuracy and robustness. Then, the solution selected the serving gNBs efficiently according to mobility preference. The corresponding signaling procedure was designed to support proactive HO processes. Simulation results showed that the proposed solution could significantly decrease the HFR and signaling cost.

References

[1] S. Chen, F. Qin, B. Hu, X. Li, and Z. Chen, "User-centric ultra-dense networks for 5G: Challenges, methodologies, and directions," *IEEE Wireless Commun.*, vol. 23, no. 2, pp. 78–85, May 2016.

[2] J. Kim, H. Lee, and S. Chong, "Virtual cell beamforming in cooperative networks," *IEEE J. Sel. Areas Commun.*, vol. 32, no. 6, pp. 1126–1138, Jun. 2014.

[3] Y. Zhang, S. Bi, and Y. A. Zhang, "User-centric joint transmission in virtual-cell-based ultra-dense networks," *IEEE Trans. Veh. Technol.*, vol. 67, no. 5, pp. 4640–4644, May 2018.

[4] N. Meng, H. Zhang, and B. Lin, "User-centric mobility management based on virtual cell in ultra-dense networks," in *Proc. IEEE/CIC Int. Conf. Commun. China*, Jul. 2016, pp. 1–6.

[5] M. Joud, M. García-Lozano, and S. Ruiz, "User specific cell clustering to improve mobility robustness in 5G ultra-dense cellular networks," in *Proc. Annu. Conf. Wireless On-Demand Netw. Syst. Services*, Feb. 2018, pp. 45–50.

[6] B. Yang, X. Yang, X. Ge, and Q. Li, "Coverage and handover analysis of ultra-dense millimeter-wave networks with control and user plane separation architecture," *IEEE Access*, vol. 6, pp. 54 739–54 750, 2018.

[7] Y. Wu, X. Fang, and X. Wang, "Mobility management through scalable C/U-plane decoupling in IoV networks," *IEEE Commun. Mag.*, vol. 57, no. 2, pp. 122–129, Feb. 2019.

[8] T. D. Assefa, R. Hoque, E. Tragos, and X. Dimitropoulos, "SDN-based local mobility management with X2-interface in femtocell networks," in *Proc. IEEE Int. Workshop Comput. Aided Model. Des. Commun. Links Netw.*, Jun. 2017, pp. 1–6.

[9] K. Wang, Y. Wang, D. Zeng, and S. Guo, "An SDN-based architecture for next-generation wireless networks," *IEEE Wireless Commun.*, vol. 24, no. 1, pp. 25–31, Feb. 2017.

[10] S. Costanzo, R. Shrivastava, D. Xenakis, K. Samdanis, D. Grace, and L. Merakos, "An SDN-based virtual cell framework for enhancing the QoE in TD-LTE pico cells," in *Proc. Int. Workshop Qual. Multimedia Exp.*, May 2015, pp. 1–6.

[11] T. Sahin, M. Klugel, C. Zhou, and W. Kellerer, "Virtual cells for 5G V2X communications," *IEEE Commun. Standards Mag.*, vol. 2, no. 1, pp. 22–28, Mar. 2018.

[12] K. Chen, T. Zhang, R. D. Gitlin, and G. Fettweis, "Ultra-low latency mobile networking," *IEEE Netw.*, vol. 33, no. 2, pp. 181–187, Mar. 2019.

[13] C. Lin, K. Chen, D. Wickramasuriya, S. Lien, and R. D. Gitlin, "Anticipatory mobility management by big data analytics for ultra-low latency mobile networking," in *Proc. IEEE Int. Conf. Commun.*, May 2018, pp. 1–7.

[14] A. I. Saleh, M. S. Elkasas, and A. A. Hamza, "Ant colony prediction by using sectorized diurnal mobility model for handover management in PCS networks," *Wireless Netw.*, vol. 25, no. 2, pp. 765–775, Feb. 2019.

[15] O. AlFarraj, A. Tolba, S. Alkhalaf, and A. AlZubi, "Neighbor predictive adaptive handoff algorithm for improving mobility management in VANETs," *Comput. Netw.*, vol. 151, pp. 224–231, May 2019.

[16] I. T. Abdel-Halim, H. M. A. Fahmy, and A. M. Bahaa-El Din, "Mobility prediction-based efficient clustering scheme for connected and automated vehicles in VANETs," *Comput. Netw.*, vol. 150, pp. 217–233, Feb. 2019.

[17] N. Meng, H. Zhang, and H. Lu, "Virtual cell-based mobility enhancement and performance evaluation in ultra-dense networks," in *Proc. IEEE Wireless Commun. Netw. Conf.*, Apr. 2016, pp. 1–6.

[18] D. S. Wickramasuriya, C. A. Perumalla, K. Davaslioglu, and R. D. Gitlin, "Base station prediction and proactive mobility management in virtual cells using recurrent neural networks," in *Proc. IEEE Wireless Microw. Technol. Conf.*, Apr. 2017, pp. 1–6.

[19] L. N. Balico *et al.*, "Localization prediction in vehicular Ad Hoc networks," *IEEE Commun. Surv. Tut.*, vol. 20, no. 4, pp. 2784–2803, May 2018.

[20] C. Randell, C. Djiallis, and H. Muller, "Personal position measurement using dead reckoning," in *Proc. IEEE Int. Symp. Wearable Comput.*, Oct. 2003, pp. 166–173.

[21] A. Agarwal and S. R. Das, "Dead reckoning in mobile Ad Hoc networks," in *Proc. IEEE Wireless Commun. Netw.*, Mar. 2003, pp. 1838–1843.

[22] F. Tang, Y. Kawamoto, N. Kato, and J. Liu, "Future intelligent and secure vehicular network toward 6G: Machine-learning approaches," *Proc. IEEE*, vol. 108, no. 2, pp. 292–307, Feb. 2020.

[23] A. Rezaei and J. B. Burl, "Prediction of vehicle velocity for model predictive control," *IFAC-PapersOnLine*, vol. 48, no. 15, pp. 257–262, Jan. 2015.

[24] S. H. Chen, C. W. Hsu, and S. C. Huang, "Recursive estimation of vehicle position by using navigation sensor fusion," in *Proc. IEEE Int. Conf. ITS Telecommun.*, Nov. 2012, pp. 532–536.

[25] R. Izquierdo, I. Parra, J. Muñoz-Bulnes, D. Fernández-Llorca, and M. A. Sotelo, "Vehicle trajectory and lane change prediction using ANN and SVM classifiers," in *Proc. IEEE Int. Conf. Intell. Transp. Syst.*, Oct. 2017, pp. 1–6.

[26] H. Woo *et al.*, "Lane-change detection based on vehicle-trajectory prediction," *IEEE Robot. Autom. Lett.*, vol. 2, no. 2, pp. 1109–1116, Apr. 2017.

[27] S. Adusumilli, D. Bhatt, H. Wang, P. Bhattacharya, and V. Devabhaktuni, "A low-cost INS/GPS integration methodology based on random forest regression," *Expert Syst. Appl.*, vol. 40, no. 11, pp. 4653–4659, Sep. 2013.

[28] H. T. Lam, E. Diaz-Aviles, A. Pascale, Y. Gkoufas, and B. Chen, "(Blue) Taxi destination and trip time prediction from partial trajectories," in *Proc. 2015th Int. Conf. ECML PKDD Discovery Challenge - Volume 1526*, ECMLPKDDDC'15, Porto, Portugal, 2015, pp. 63–74.

[29] H. Zhang and L. Dai, "Mobility prediction: A survey on state-of-the-art schemes and future applications," *IEEE Access*, vol. 7, pp. 802–822, 2018.

[30] L. N. Balico, H. A. Oliveira, E. L. Souza, R. W. Pazzi, and E. F. Nakamura, "On the performance of localization prediction methods for vehicular ad hoc networks," in *Proc. IEEE Symp. Comput. Commun.*, Jul. 2015, pp. 359–364.

[31] K. Liu, Z. Asher, X. Gong, M. Huang, and I. Kolmanovsky, "Vehicle velocity prediction and energy management strategy part 1: Deterministic and stochastic vehicle velocity prediction using machine learning," *SAE Tech. Pap.*, Warrendale, PA, USA, 2019, doi: 10.4271/2019-01-1051.

[32] X. Song, H. Kanasugi, and R. Shibasaki, "Deeptransport: Prediction and simulation of human mobility and transportation mode at a citywide level," in *Proc. Int. Joint Conf. Artif. Intell. Org.*, vol. 16, Jul. 2016, pp. 2618–2624.

[33] S. Hochreiter and J. Schmidhuber, "LSTM can solve hard long time lag problems," in *Proc. Advances Neural Inf. Process. Syst.*, Dec. 1997, pp. 473–479.

[34] F. A. Gers, J. Schmidhuber, and F. Cummins, "Learning to forget: Continual prediction with LSTM," in *Proc. Int. Conf. Artif. Neural Netw.*, Sep. 1999, pp. 850–855.

[35] F. Altché and A. de La Fortelle, "An LSTM network for highway trajectory prediction," in *Proc. IEEE Int. Conf. Intell. Transp. Syst.*, Oct. 2017, pp. 353–359.

[36] W. Liu and Y. Shoji, "Applying deep recurrent neural network to predict vehicle mobility," in *Proc. IEEE Veh. Netw. Conf.*, Dec. 2018, pp. 1–6.

[37] J. Xu, R. Rahmatizadeh, L. Bölöni, and D. Turgut, "Real-time prediction of taxi demand using recurrent neural networks," *IEEE Trans. Intell. Transp. Syst.*, vol. 19, no. 8, pp. 2572–2581, Aug. 2018.

[38] B. Hassibi and B. M. Hochwald, "How much training is needed in multiple-antenna wireless links?" *IEEE Trans. Inf. Theory*, vol. 49, no. 4, pp. 951–963, Apr. 2003.

[39] A. M. Alam, P. Mary, J. Baudais, and X. Lagrange, "Energy efficiency-area spectral efficiency tradeoff in PPP network with SLNR precoder," in *Proc. IEEE Int. Workshop Signal Process. Advances Wireless Commun.*, Jul. 2016, pp. 1–6.

[40] R. Tanbourgi, S. Singh, J. G. Andrews, and F. K. Jondral, "A tractable model for noncoherent joint-transmission base station cooperation," *IEEE Trans. Wireless Commun.*, vol. 13, no. 9, pp. 4959–4973, Sep. 2014.

[41] Q. Liu, G. Chuai, W. Gao, and K. Zhang, "Fuzzy logic-based virtual cell design in ultra-dense networks," *EURASIP J. Wireless Commun. Netw.*, vol. 2018, no. 1, pp. 87–100, Apr. 2018.

[42] L. Bracciale, M. Bonola, P. Loreti, G. Bianchi, R. Amici, and A. Rabuffi, "CRAWDAD dataset Roma/taxi (v. 2014-07-17)," Jul. 2014. [Online]. Available: https://crawdad.org/roma/taxi/20140717

[43] F. V. Baumann and I. G. Niemegeers, "An evaluation of location management procedures," in *Proc. IEEE Int. Conf. Universal Personal Commun.*, Sep. 1994, pp. 359–364.

[44] Q. Liu, G. Chuai, J. Wang, J. Pan, W. Gao, and X. Liu, "Proactive mobility management based on virtual cells in SDN-enabled ultra-dense networks," in *Proc. IEEE Int. Conf. Commun. Workshops*, May 2019, pp. 1–6.

Qian Liu received the M.Sc. degree in communication and information systems from the Kunming University of Science and Technology, in 2013. She is currently working toward the Ph.D. degree in information and communications engineering with the Beijing University of Posts and Telecommunications (BUPT), Beijing, China. From 2018 to 2020, she was a Visiting Ph.D. Student with the University of Victoria, Victoria, Canada. Her research interests include ultra-dense networks, virtual cells, and modeling and analysis of cellular networks using stochastic geometry.

Gang Chuai received the M.Sc. and Ph.D. degrees in information and communications engineering with the Beijing University of Posts and Telecommunications (BUPT), Beijing, China, in 1999 and 2010, respectively. He is currently the Full Professor with the School of Information and Communication Engineering, BUPT. From 2006 to 2007, he was a Senior Visiting Scholar with the University of Drexel, Philadelphia, USA. His main research interests include wireless communications networking technology, intelligent network optimization, dynamic performance analysis of wireless network, and wireless network positioning theory.

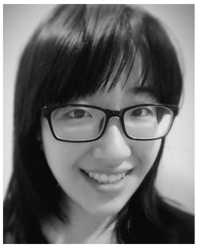

Jingrong Wang (Student Member, IEEE) received the bachelor's degree from the School of Electronic and Information Engineering, Beijing Jiaotong University in, 2017, and the M.Sc degree in computer science from the University of Victoria, in 2019. She is currently working toward the Ph.D. degree at the University of Toronto. Her research interests cover wireless communications, mobile edge computing, and distributed machine learning.

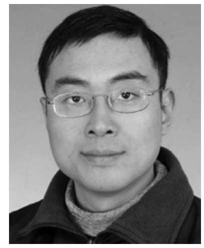

Jianping Pan (Senior Member, IEEE) received the bachelor's and Ph.D. degrees in computer science from Southeast University, Nanjing, Jiangsu, China. He is currently a Professor of computer science with the University of Victoria, Victoria, British Columbia, Canada. He did his postdoctoral research with the University of Waterloo, Waterloo, Ontario, Canada. He also worked with Fujitsu Labs and NTT Labs. His area of specialization is computer networks and distributed systems, and his research interests include protocols for advanced networking, performance analysis of networked systems, and applied network security. He received the IEICE Best Paper Award in 2009, the Telecommunications Advancement Foundation's Telesys Award in 2010, the WCSP 2011 Best Paper Award, the IEEE Globecom 2011 Best Paper Award, the JSPS Invitation Fellowship in 2012, the IEEE ICC 2013 Best Paper Award, and the NSERC DAS Award in 2016, and is a coauthor of one of the three IEEE LCN 2018 Best Paper Award candidates, and has been serving on the technical program committees of major computer communications and networking conferences including IEEE INFOCOM, ICC, Globecom, WCNC, and CCNC. He was the Ad Hoc and Sensor Networking Symposium Co-Chair of IEEE Globecom 2012 and an Associate Editor of the IEEE TRANSACTIONS ON VEHICULAR TECHNOLOGY.